ADVANCES IN APPLIED MATHEMATICS 10, 201–227 (1989)

The Interaction of Shock Waves with Fluid Interfaces

JOHN GROVE*

Courant Institute of Mathematical Sciences, New York University, New York, New York 10012

Enhanced resolution for the computation of the interaction of shock waves with fluid interfaces is achieved through a detailed mathematical analysis of 2-dimensional wave interactions produced during the collision of the waves. This computation is carried to late times, which are characterized by interface instability and chaotic mixing processes. Algorithms for incorporating the wave interaction analysis and the resulting bifurcation of front topology give an important extension of the front tracking method and are presented here. The mathematical analysis shows that the customary theory for oblique 2-dimensional wave interactions is equivalent to a 1-dimensional Riemann problem for steady (supersonic) flow. This analysis, known for polytropic gases, is extended here to a general equation of state. Moreover, the asymptotic limit of a small incident angle is analyzed to obtain a well-conditioned numerical algorithm. This limit is found to define a 1-dimensional unsteady Riemann problem.

1. INTRODUCTION

There are two distinct time periods for the analysis of the interaction of a shock wave with a fluid interface. In the short time periods 2-dimensional wave interactions and bifurcations of front topology dominate the problem. Over a longer time period, interface instability, entrainment, and chaotic mixing are the major phenomena.

The main thrust of the paper is to use a detailed mathematical analysis of the short term 2-dimensional wave interactions to give enhanced resolution computations of long term mixing processes. Enhanced resolution is obtained through the front tracking algorithm [8, 12–14]. The enhanced

*Supported in part by the Army Research Office Grant DAAG29-84-K-0130.

0196-8858/89 $7.50

resolution appears to be at least a factor of 4.4 per linear dimension, or 85 per space time grid block, compared to other methods. An important extension of this method is required for the problems considered here.

The shock–contact interaction problem presents a level of complexity in the fluid flow not previously handled by the front tracking method. The required extension of the method to deal with such problems is among the principal new results reported in this paper. These results are achieved by carrying out a mathematical analysis of the 2-dimensional interaction of shock waves with fluid interfaces and incorporating this information directly into the computational process. The application of this procedure to numerical studies of shock–contact interactions, as reported here, constitutes a proof of principle for the front tracking method in the present context.

The mathematical analysis begins with the observation that the cumbersome shock polar analysis for oblique 2-dimensional wave interactions can be interpreted as a 1-dimensional Riemann problem for steady (supersonic) flow. The customary analysis of this problem, valid for polytropic gases, is extended to a general equation of state. This extension, while not needed for the computational examples presented here, will be required for a subsequent comparison of computation with experiment. It is also shown that for large flow speeds, the steady state Riemann problem has a 1-dimensional Riemann problem as an asymptotic limit. The analysis of this asymptotic limit was necessary to obtain a well-conditioned algorithm in the limit of small incident angles.

A further contribution of this paper is to describe the algorithms for incorporating bifurcations of front topology into the front tracking computation. These algorithms generalize previous bifurcation algorithms obtained for the case of scalar waves [16]. Computational examples are presented.

Chaotic mixing caused by the acceleration of a fluid interface by a shock wave is known as the Richtmyer–Meshkov instability [6, 26]. Recent calculations of D. L. Youngs [34] use a volume in cell Eulerian method [17, 24, 25, 33] with the monotonic advection method of Van Leer [19, 20] to enhance the interface resolution and to minimize the numerical diffusion. His problems are not exactly comparable to the ones presented here, but it appears that the front tracking method gives an increased resolution by a factor of at least 4.4 per linear dimension. Comparisons of front tracking in the context of other problems, with the solutions obtained using different numerical methods, show increased resolutions by factors of up to 3–5 per linear dimension, or 27–125 per space time grid block. One extreme case showed an increased resolution of 50 per linear dimension, or $50^3 = 1.25 \times 10^6$ per space time grid block [15].

2. The Equations of Motion and Thermodynamic Preliminaries

The equations of motion are the Euler equations in two space dimensions for a non-viscous, non-heat conducting gas:

$$\partial_t \rho + \nabla \cdot (\rho \mathbf{q}) = 0, \tag{2.1.1}$$

$$\partial_t (\rho \mathbf{q}) + \nabla \cdot (\rho \mathbf{q} \otimes \mathbf{q}) + \nabla P = 0, \tag{2.1.2}$$

$$\partial_t (\rho \mathscr{E}) + \nabla \cdot ((\rho \mathscr{E} + P)\mathbf{q}) = 0. \tag{2.1.3}$$

Here $\mathbf{q}$ is the particle velocity, ρ is the mass density, P is the thermodynamic pressure, $\mathscr{E} = |\mathbf{q}|^2/2 + E$ is the specific total energy, and E is the specific internal energy.

System (2.1) is closed by a caloric equation of state

$$E = E(V, S) \tag{2.2}$$

expressing the specific internal energy as a function of the specific volume $V = 1/\rho$, and the specific entropy S. The equation of state represents the response of the fluid to changes in temperature and volume and is restricted by the laws of physics. In particular, $E(V, S)$ satisfies the first law of thermodynamics,

$$T\,dS = dE + P\,dV, \tag{2.3}$$

where T is the absolute temperature. The assumption that the fluid remains in stable thermodynamic equilibrium implies that $E(V, S)$ is convex [32]. This implies that the sound speed $c^2 = (\partial P/\partial \rho)|_S$ is real, and P is monotone in V for constant S. Other restrictions on $E(V, S)$ that govern the monotonicity and asymptotic properties of the wave curves for (2.1) are derived in [27, 23], and will be assumed when necessary. These added assumptions supply sufficient conditions for the existence and uniqueness of the solution to the one dimensional unsteady Riemann problem.

3. Dimensional Reduction for 2-Dimensional Elementary Wave Interactions

An elementary wave is by definition a steady, scale invariant solution of a system of hyperbolic conservation laws [10, 11, 14]. It consists of discrete waves moving at a constant velocity. According to the streamline directions, these waves are defined as either incoming or outgoing.

The analysis presented in the next two sections will consider the case where the elementary wave consists of two incoming waves with supersonic states on their downstream edges. The task in studying such elementary

waves is to determine the outgoing waves, while the incoming waves are regarded as data. In hydrodynamics these waves include the crossing of two shock waves, the overtaking of one shock by another, and the diffraction of a shock at a fluid interface [14]. Other elementary waves include a Mach triple point and the interaction of several contact discontinuities.

This section starts with the new observation that the outgoing waves are determined as solutions of a 1-dimensional Riemann problem, namely that defined for steady state 2-dimensional flow (with the stream direction as a "time" axis). This point of view is equivalent to the more conventional description of such wave interactions by the intersection of shock polars, but has the advantage of greater mathematical clarity. It unifies the role of simple waves and shocks in the solution and stresses the analogy between the solution to such problems and the Riemann problem for 1-dimensional unsteady flow. The main result here is built on this observation. The existence of a solution to the steady 2-dimensional Riemann problem for large flow speeds and a general equation of state is demonstrated below. This existence result carries over to the corresponding statement for 2-dimensional elementary waves. In general such solutions are not unique. However, it will be seen that the leading order asymptotic behavior for large flow speeds of the supersonic steady problem is the 1-dimensional unsteady problem. The lowest pressure (highest Mach number) solution to the 2-dimensional steady Riemann problem is the asymptotically "correct" solution. This fact agrees with the experimental observation of Henderson [1–3, 5], that the lowest pressure solution to the shock polar analysis is the one observed experimentally.

Each "supersonic" elementary wave can be viewed as the downstream scattering of the interacting incoming waves. The two incoming waves set up a pair of supersonic states that serve as upstream "initial" conditions for the downstream flow. It is in this sense that the downstream scattering of the incoming waves is the solution to a Riemann problem.

4. The Wave Analysis for a General Equation of State

Before continuing with this discussion, it is necessary to summarize the wave analysis of steady planar flow. This discussion is based on the analysis of a general system of hyperbolic conservation laws [18]. In the following q and θ are the polar coordinates of the stream velocity $\mathbf{q}$.

The restriction of (2.1) to steady planar flow yields a system of four conservation laws in the two space variables x and y. This system is non-strictly hyperbolic for supersonic flow. It has three families of characteristics. The middle family, denoted C_0, is a linearly degenerate mode of double multiplicity, with characteristic direction given by the streamlines

$dx = \cos\theta$ and $dy = \sin\theta$. The waves of this family are contact discontinuities (slip lines) where the pressure and flow angle are continuous and the density and flow speed may experience jumps. The linear degeneracy of this family implies that the solution to the Riemann problem for steady planar flow reduces to finding the intersection of the wave curves of the remaining two families in the (P, θ) phase plane. The flow angle θ is the natural analogue of the particle speed in the solution to the 1-dimensional unsteady Riemann problem.

The two other characteristic families, denoted $C_{\pm}$, are associated with the propagation of sound waves. These characteristics cross the streamlines with the Mach angle A ($\sin A = c/q$) and have characteristic directions $dx = \cos(\theta \pm A)$ and $dy = \sin(\theta \pm A)$, respectively. These characteristics are genuinely nonlinear if and only if the fundamental derivative of gas dynamics

$$\mathcal{G} = -\frac{V}{2}\frac{\partial^3 E/\partial V^3|_S}{\partial^2 E/\partial V^2|_S} \tag{4.1}$$

does not vanish [28, 29]. For real materials, $\mathcal{G} > 0$ at most pressures and temperatures, but $\mathcal{G}$ may be negative for some values of P and T, in particular near phase transitions. The case where $\mathcal{G}$ is not strictly positive allows the introduction of considerably more complicated wave behavior and will be discussed in a future paper. In the following $\mathcal{G}$ is assumed to be positive.

The Rankine–Hugoniot relations for a stationary oblique shock are [9, pp. 297–302]:

$$E_1 - E_0 = \frac{(P_1 + P_2)}{2}(V_0 - V_1), \tag{4.2.1}$$

$$\frac{q_0^2}{2} + H_0 = \frac{q_1^2}{2} + H_1, \tag{4.2.2}$$

$$(P_1 - P_0)(V_0 - V_1) = (\mathbf{q}_0 - \mathbf{q}_1)^2, \tag{4.2.3}$$

$$(\mathbf{q}_0 - \mathbf{q}_1) \cdot \mathbf{T} = 0. \tag{4.2.4}$$

Here $\mathbf{T}$ is a unit vector parallel to the oblique shock, and the subscripts 0 and 1 refer to the states on the upstream and downstream sides of the shock wave, respectively.

If β_i denotes the angle between the oblique shock front and the flow vector $\mathbf{q}_i$, and $m^2 \equiv (P - P_0)/(V_0 - V)$ is the mass flux across the oblique shock, then (4.2.3) and (4.2.4) can be replaced by the equivalent relations:

$$\tan(\theta_1 - \theta_0) = \left[\frac{P_1 - P_0}{\rho_0 q_0^2 - (P_1 - P_0)}\right]\cot \beta_0, \tag{4.2.5}$$

$$\sin^2 \beta_i = \frac{m^2}{\rho_i^2 q_i^2}. \tag{4.2.6}$$

For a fixed upstream state, (4.2.5) defines a locus of points in the pressure-flow angle phase space known as the (θ, P) shock polar.

Equation (4.2.1) is the Hugoniot relation and is of particular importance since it involves only thermodynamic quantities. The properties of the Hugoniot locus of solutions to (4.2.1) are discussed in [7, 23, 27, 31]. Some properties of the Hugoniot locus are given by the following theorem [23].

THEOREM 1 (Bethe, Weyl, Menikoff, and Plohr). *The Hugoniot locus through an initial state (V_0, S_0) intersects each isentrope at least once. If in addition $\mathcal{G} > 0$, then the Hugoniot locus intersects each isentrope exactly once and $(S - S_0)(V_0 - V) > 0$ for $S \neq S_0$. Moreover, m is real, finite, and monotone along the Hugoniot, and 1-dimensional shocks satisfy the Lax stability condition.*

Theorem 1 has important consequences for the analysis of the Riemann problem. A new observation is that for a general equation of state with suitable asymptotic restrictions on the pressure, the (θ, P) shock polars form closed and bounded loops if $\mathcal{G} > 0$. This generalizes the previously known result for the polytropic equation of state.

PROPOSITION 1. *Assume that $\mathcal{G} > 0$ and the pressure satisfies the asymptotic condition $P(V, S) \to \infty$ as $S \to \infty$. Then the state upstream of a steady oblique shock wave is supersonic, and the (θ, P) shock polar through this point is a single closed connected loop.*

Proof. Since the entropy across a physical shock may not decrease, Theorem 1 implies that if $\mathcal{G} > 0$, shocks are compressive and the compressive branch of the Hugoniot can be parameterized by the entropy $S > S_0$. Differentiating (4.2.1) and applying (2.3) shows that along the shock Hugoniot

$$dm^2 = \frac{2T\,dS}{(V_0 - V)^2} \geq 0. \tag{4.3}$$

Clearly (4.2.6) has a real solution if and only if $\rho_0^2 q_0^2 \geq m^2$. The Lax stability condition is equivalent to the inequalities, valid along the shock

Hugoniot, $\rho_0 c_0 < m < \rho c$ when $V < V_0$, and $\rho_0 c_0 > m > \rho c$ when $V > V_0$. Since the entropy is nondecreasing across a shock, $m > \rho_0 c_0$, and the state upstream of the shock is supersonic. Next, note that $m^2 > (P(V_0, S) - P_0)/V_0$, for $V < V_0$. Thus along the shock Hugoniot, $m^2 \to \infty$ as $S \to \infty$. Therefore (4.2.6) has no real solutions for large P. Finally, the monotonicity of m^2 along the Hugoniot implies that the shock polar consists of a single connected loop. □

The (θ, P) shock polar has two symmetric branches. If $\mathcal{G} > 0$, these two branches meet at a point in the (θ, P) plane where the shock is normal to the streamlines. Since the flow downstream from a weak oblique shock is supersonic and the flow downstream from a normal shock is subsonic, the solution to the Riemann problem can be transonic.

The non-monotonicity of the Hugoniots in the (θ, P) phase plane can lead to a loss of existence or uniqueness of the solution to the Riemann problem. Nonexistence means that steady upstream data can lead to unsteady flow downstream. Non-uniqueness is not just mathematical and may depend on downstream boundary conditions [9, pp. 317–318].

These observations show that the Riemann problem for steady flow is considerably more non-linear and complicated than that of 1-dimensional unsteady flow. They also show that the general Riemann problem for steady flow must be studied in the context of a full dimensional unsteady flow.

Another consequence of Theorem 1 is the steady state version of the Lax shock admissibility criterion.

PROPOSITION 2. *Assume* $\mathcal{G} > 0$. *If all angles are normalized to lie in the interval* $(-\pi/2, \pi/2)$, *then* $|\beta_1| < |\beta_0|$ *and* $A_0 < |\beta_0|$. *If the downstream state is supersonic, then* $A_1 > |\beta_1|$.

Proof. Equation (4.2.6) is equivalent to the equation $\sin|\beta_i| \equiv (m/\rho_i c_i)(1/M_i)$. Since $\sin A_i = 1/M_i$ if $M_i \geq 1$, the inequalities between Mach and shock angles follow immediately. The inequality between the two shock angles is a consequence of the equality $\rho_1 \tan|\beta_1| = \rho_0 \tan|\beta_0|$, that can be derived from (4.2.1), (4.2.2), and (4.2.6). □

This is the steady state version of the Lax shock stability criterion since if $A_0 < |\beta_0|$, then each of the characteristics on the upstream side of the oblique shock flow into the wave. If the state downstream from the shock is supersonic, then $A_1 > |\beta_1|$ implies that exactly one downstream characteristic flows into the shock from the upstream direction, and the other two downstream characteristics flow away from the shock.

Proposition 2 shows that shock waves that turn the flow in the positive (counterclockwise) direction belong to the C_+ characteristic family in the sense of Lax, and those with negative turning angles belong to the C_- characteristic family.

The simple waves of the $C_{\pm}$ families are the well known Prandtl–Meyer rarefaction waves. Prandtl–Meyer waves are isentropic, so the pressure is monotone along the wave curve and can be used to parameterize that curve. A straightforward but tedious calculation shows that the $C_{\pm}$ simple wave curve through the state $\mathbf{w}_0$ is given by

$$q^2(P, \mathbf{w}_0) = q_0^2 + 2(H(P_0, S_0) - H(P, S_0)), \tag{4.4.1}$$

$$\theta(P, \mathbf{w}_0) = \theta_0 \pm \int_{P_0}^{P} \frac{\cos A}{q} \frac{dp}{c\rho}, \tag{4.4.2}$$

$$S(P, \mathbf{w}_0) = S_0. \tag{4.4.3}$$

Here $H = E + PV$ is the specific enthalpy.

The wave curve through a given state is the concatenation of the compressive branch of the shock Hugoniot through that state with the rarefaction portion of the simple wave curve. In applications it is common

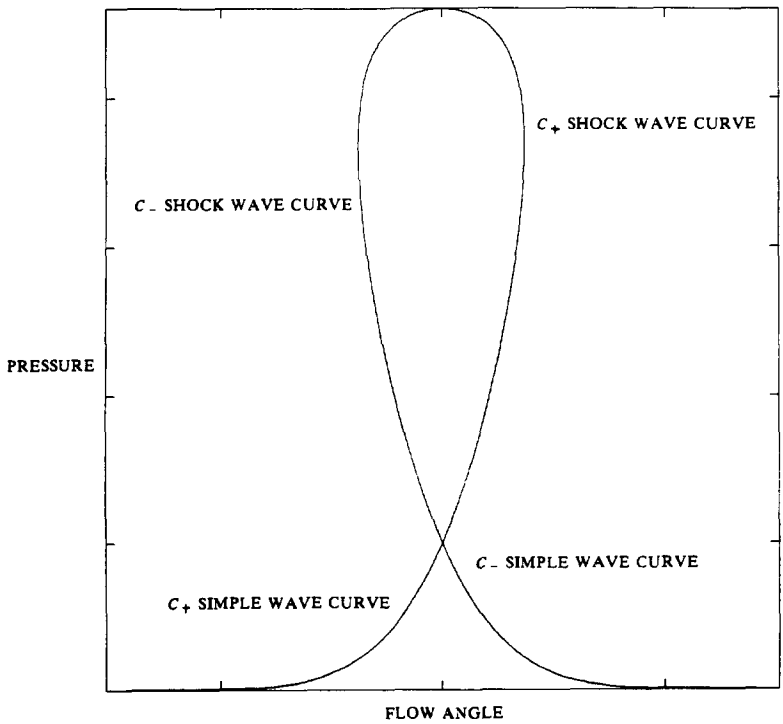

FIG. 4.1. A representative wave curve for supersonic steady flow showing the (θ, P) shock polar together with the simple wave curves for a Prandtl–Meyer rarefaction fan.

to parameterize this curve by pressure. This is always possible for the rarefaction branch, but the pressure need not be monotone along the Hugoniot for a general equation of state. A sufficient condition for the monotonicity of the pressure along the shock Hugoniot is the inequality $\Gamma \leq 2\gamma$, [23, 27]. Here γ is the adiabatic exponent, $\gamma = -(\partial \log P/\partial \log V)|_S$, and Γ is the Grüneisen coefficient, $\Gamma = -(\partial \log T/\partial \log V)|_S$. This inequality, known as the WEAK condition, is valid for most real equations of state and is assumed in the following. Figure 4.1 shows a representative (θ, P) wave curve.

5. Large Flow Speed Asymptotics of the Steady Euler Equations

This section will analyze the asymptotic limit of the steady state Riemann problem as the flow speed goes to infinity. The main point of this section is that as the flow speed becomes large, a steady oblique wave converges under a Galilean transformation to a 1-dimensional unsteady wave. This is a consequence of the Galilean invariance of the Euler equations and the scale invariance of solutions to the Riemann problem. For simplicity, suppose that the upstream velocity is parallel to the positive x axis. A self-similar solution to the steady state Euler equations is a function of $\eta = y/x$. If $\mathbf{F}$ and $\mathbf{G}$ are the spatial fluxes in (2.1), the solution $\mathbf{w}(\eta)$ satisfies the characteristic equation $(d\mathbf{G} - \eta\, d\mathbf{F})\mathbf{w}'(\eta) = 0$. If $\hat{\mathbf{w}}$ is the image of $\mathbf{w}$ under the Galilean transform $\hat{x} = x - q_0 t$, then $\hat{\mathbf{w}}$ is a function of $\xi = q_0 y/(\hat{x} + q_0 t)$ and also solves the Euler equations. If $\mathbf{U}$ is the time flux in (2.1), then $(d\mathbf{G} - \xi\, d\mathbf{U} - \xi\, d\mathbf{F}/q_0)\hat{\mathbf{w}}'(\xi) = 0$. As $q_0 \to \infty$, the equation for $\hat{\mathbf{w}}$ converges to the solution of a 1-dimensional unsteady scale invariant flow. A similar statement applies for the Rankine–Hugoniot equations.

In somewhat more detail, the wave curve for the unsteady 1-dimensional Euler equations through the state with velocity v_0, is $v = v_0 \pm \phi(P, P_0, S_0)$, where $\phi(P, P_0, S_0) = [(P - P_0)(V_0 - V)]^{1/2}$ for $P > P_0$, and $\int_{P_0}^{P} (dP/c\rho)|_{S=S_0}$ for $P < P_0$. The 2-dimensional steady wave curve through the state with velocity $\mathbf{q}_0$, and the same pressure and entropy is given by $\theta = \theta_0 \pm \psi(P, q_0, P_0, S_0)$, where ψ is defined by (4.2.5) for $P > P_0$ and (4.4.2) for $P < P_0$. If P is less than the maximum pressure $P_{\max}(q_0)$ on the (θ, P) shock polar, then $\psi(P, q_0, P_0, S_0) = (\phi(P, P_0, S_0)/q_0)(1 + O(1/q_0^2))$ and the downstream flow speed q satisfies $q = q_0(1 + O(1/q_0^2))$. Furthermore, $P_{\max}(q_0) \to \infty$ as $q_0 \to \infty$, and for each $P_1 > P_0$, the $O(1/q_0^2)$ terms coverage uniformly to zero for $0 \leq P \leq P_1$ as $q_0 \to \infty$. Thus under this Galilean transformation, the steady planar flow wave curve converges to the 1-dimensional unsteady wave curve.

This reasoning can be used to prove the following theorem.

THEOREM 2. *Suppose that for the given equation of state, the solution to the* 1*-dimensional Riemann exists and is unique. Let* $\mathbf{q}_0(\beta)$ *and* $\mathbf{q}_1(\beta)$ *be a family of flow velocities. Suppose that*

1. *there is a vector* $\mathbf{e}$ *so that* $\mathbf{q}_i \cdot \mathbf{e}$ *tends to a finite limit* v_i *as* $\beta \to 0$,
2. $\lim_{\beta \to 0} q_i = \infty$,
3. $\lim_{\beta \to 0}(q_0/q_1) = 1$.

Then the steady state Riemann problem with data $(\mathbf{q}_0(\beta), P_0, S_0)$ *and* $(\mathbf{q}_1(\beta), P_1, S_1)$ *has a self-similar solution for* β *sufficiently small. If* $P(\beta)$ *is the pressure of the lowest pressure solution to this steady state Riemann problem, then* $P(\beta)$ *converges to the pressure* P *of the solution to the one dimensional Riemann problem with data* (v_i, P_i, S_i). *Under the Galilean transformation with velocity* $\mathbf{q}_0(\beta)$, *the steady state solution with pressure* $P(\beta)$ *converges to the solution of the unsteady problem.*

6. SHOCK–CONTACT INTERACTIONS

Representative planar shock–contact interactions are shown in Figs. 6.1, and 6.2. If the interaction is observed in a frame where the two incident waves are at rest, the upstream data defines a steady state Riemann problem for the downstream flow. A shock–contact interaction is called regular if a solution to this steady state Riemann problem exists and consists of the usual three downstream propagating waves.

Irregular shock–contact diffraction configurations are also possible. These include such additional features as Mach reflections and precursor shock configurations [1, 2, 4]. A future paper will discuss methods for modeling these more complicated configurations.

The next theorem shows that for small incident angles it is enough to model the regular case.

THEOREM 3. *Assume the equation of state satisfies sufficient conditions for the existence and uniqueness of the* 1*-dimensional unsteady Riemann problem. Then for a given incident shock strength, the regular diffraction pattern occurs provided the angle between the incident shock wave and the contact discontinuity is sufficiently small. Furthermore, the transmitted wave is a shock.*

Proof. The proof is the observation that the conditions of Theorem 2 are satisfied as the incident angle goes to zero. For simplicity suppose that in the lab frame, the gases ahead of the interaction are at rest. If the upstream contact lies along the positive x-axis and the shock is incident from above, then the incident angle β is positive. The steady state upstream velocities in the frame where the two incident waves are at rest are given by

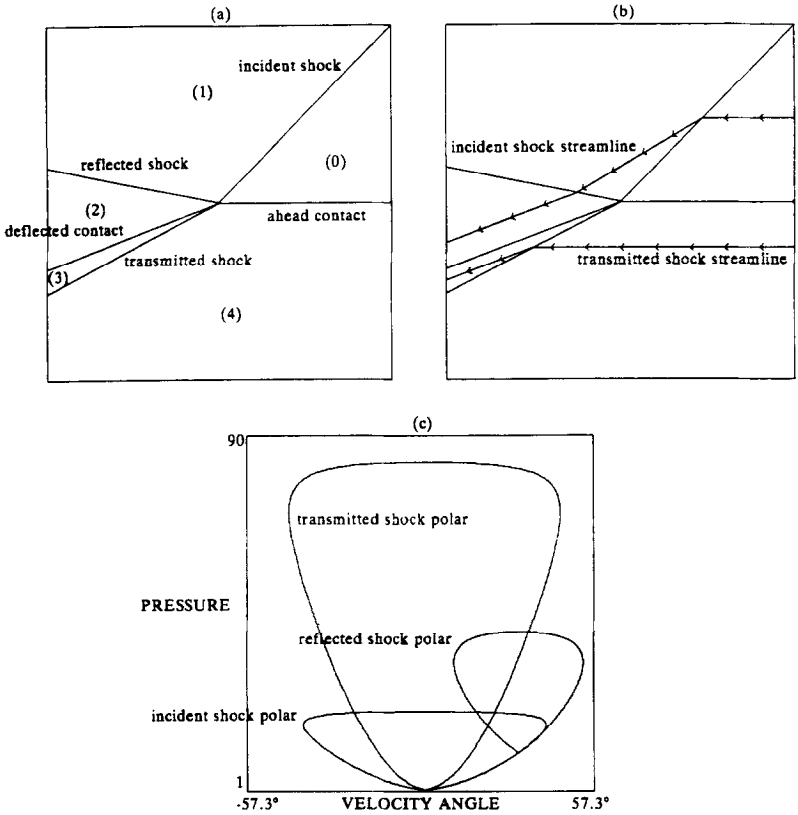

FIG. 6.1. A shock wave–contact discontinuity collision that produces a single reflected shock. The two gases are polytropic with $\gamma = 1.402$. The gas on the transmitted shock side of the ahead contact discontinuity is four times as dense as the gas on the incident shock side. The angle between the incident shock and the ahead contact discontinuity is 45°, and the ratio of the pressures across the incident shock is 10. The flow is turned by about 30.3° through the incident shock, −9.8° through the reflected shock, and 20.5° through the transmitted shock.

$\mathbf{q}_0 = \mathbf{q}_1 = \langle -q_1, 0\rangle$, where $q_1 \sin \beta = m/\rho_1$. Here the subscripts 0 and 1 refer to the states of the gas on the two sides of the upstream contact. The shock is incident on the gas with state 1. Let state 2 be the state behind the incident shock. Note that the thermodynamics of these three states are independent of β. The solution to the regular diffraction is the solution to the steady state Riemann problem with data states 0 and 2. The result will follow once conditions 1–3 of Theorem 2 are verified. This is trivial for state 0. To check these conditions for state 2 let $\mathbf{q}_2 = \langle u_2, v_2\rangle$. A little algebra applied to (4.2) shows that $u_2 = -(m/\rho_0)\csc\beta(1 + O(\beta))$ and $v_2 = -[(P_2 - P_1)(V_1 - V_2)]^{1/2}(1 + O(\beta))$. The final statement is a consequence of the 1-dimensional unsteady interaction and is easily verified. □

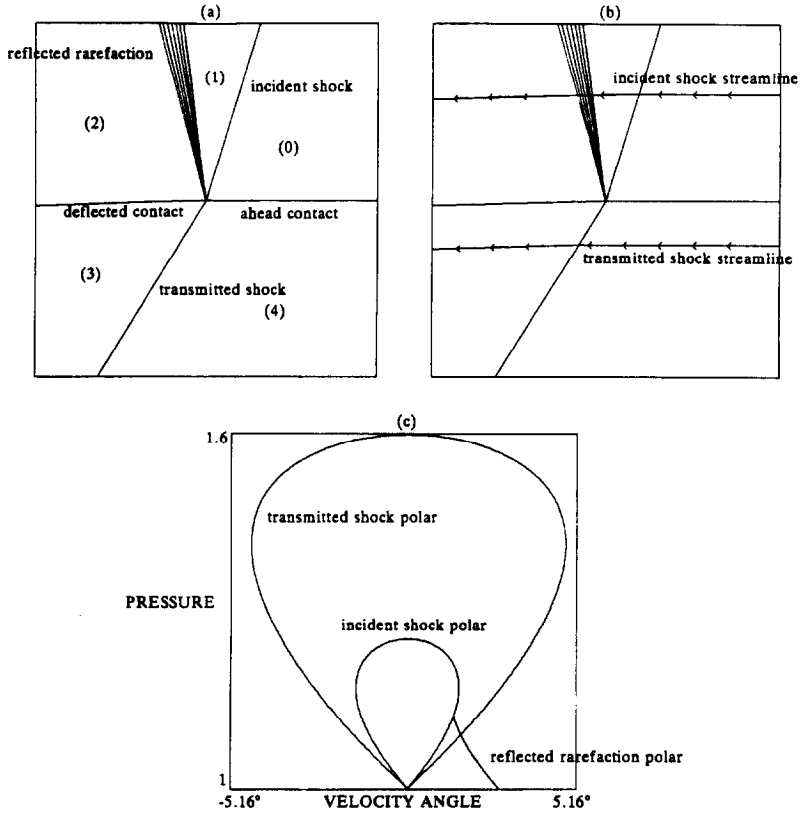

FIG. 6.2. A shock wave–contact discontinuity collision that produces a reflected Prandtl–Meyer rarefaction wave. The two gases are polytropic with $\gamma = 1.402$. The gas on the transmitted shock side of the upstream contact discontinuity is 1.24 times as dense as the gas on the incident shock side. The angle between the incident shock and the ahead contact discontinuity is 72.7°, and the ratio of the pressures across the incident shock is 1.12. The flow is turned by 1.36° through the incident shock, 0.21° through the reflected shock, and 1.57° through the transmitted shock.

This theorem has the important consequence that for the Richtmyer–Meshkov problem, irregular solutions are obtained from bifurcations of regular solutions. The two waves are tangent when they first collide, so in the early stages of the interaction the incident angle is small. Subsequently, this angle may grow to a point where the regular solution no longer exists and a bifurcation to an irregular configuration occurs. Just as for the transition from regular to Mach reflection, there may be a region where multiple solutions are possible and a transition criterion is needed to select the physical solution.

The loss of uniqueness extends to the case of regular diffractions. It is possible to have two or more regular solutions for a single steady state Riemann problem. In such cases, the solution with the lowest pressure is selected as mentioned above.

7. The Front Tracking Algorithm

The front tracking algorithm [8, 12–14], is an adaptive grid method for the sharp resolution of selected waves in numerical solutions to systems of partial differential equations in two space dimensions:

$$\mathbf{w}_t + \nabla \cdot \mathbf{F}(\mathbf{w}) = 0. \tag{7.1}$$

The tracked waves may represent sharp discontinuities in the solution such as shocks or contact discontinuities, or regions where the solution is changing rapidly such as chemical reaction fronts. The selected waves are tracked by superimposing a set of 1-dimensional curves onto an underlying rectangular grid. These curves correspond to the location of the tracked waves at a given time and are dynamically modified as the solution evolves in time. In hydrodynamics, the tracked curves include shock waves, leading and trailing edges of rarefaction waves, contact discontinuities, and boundary curves.

The solution at an interior point on a curve is propagated using local operator splitting. A 1-dimensional Riemann problem for the component of (7.1) along the normal to the curve at that point gives the updated position of the wave and a set of propagated states. Subsequently, a finite difference sweep along the tangential direction of the curve is performed to complete the propagation. Exceptional points, called nodes, occur when several curves meet at a common point. Nodes correspond to 2-dimensional elementary waves and are propagated using a fully 2-dimensional algorithm that is appropriate for each type of wave. The tracked data structures (curves and nodes), serve as internal boundaries for the solution in the untracked portion of the computation grid.

8. The Propagation of Supersonic Elementary Waves

The propagation of a node is of primary interest in this paper and is discussed in more detail. This propagation computes the time updated position and states of the node. It is distinguished from the propagation of the other points of the tracked interface since the solution is fully 2-dimensional near nodes and operator splitting into 1-dimensional components may not apply.

Briefly, each curve connected to a node contains the state information for the tangential limit of the solution as the node is approached along that curve. This information together with the one-sided tangent directions of the curves at the node define an initial value problem with data that is constant on rays centered at the node position. The solution of the initial value problem for (7.1) with scale-invariant initial data is a natural generalization of the Riemann problem for systems of hyperbolic equations in one space dimension [11].

Each node is assumed to be a first-order perturbation of an elementary wave. The solution to the associated 2-dimensional Riemann problem is approximated by the calculating the corresponding elementary wave. This elementary wave data is inserted into the tracked data structures at the node giving the time-updated states and angles of the waves at the node. Any scattered waves produced by the perturbation are captured by the interior (untracked) solution. The data for the elementary wave at the node changes with time because of curvature of incoming waves or variability of the upstream data. Thus the solution about a node dynamically evolves. The changing geometric and state data may lead to bifurcations in the node topology causing a single node to scatter into a set of waves.

The calculation of an elementary wave requires the determination of the translational velocity of the wave in the computational lab frame, i.e., the velocity of the corresponding node in the lab frame. For the "supersonic" elementary waves this velocity is determined by the states and angles of the incoming waves. In practice this velocity is computed using a geometric construction. If no bifurcation in the solution near the node occurs between times t and $t + \Delta t$, the propagated node position lies on both of the propagated incoming waves. The intersection of these curve segments determines the new node position, and the node displacement divided by Δt gives the node velocity. The upstream state data is found by linear interpolation along the intersecting segments of the propagated incoming waves. The solution of the steady state Riemann problem with this data determines the outgoing waves. The incoming waves are clipped to the new node position, and the upstream state data at the node is recorded in the incoming wave structures. The downstream information is inserted in the outgoing waves by recording the downstream states in the outgoing wave structures and inserting a point in each outgoing curve to correct the angle that the wave makes at the node. It should be mentioned that not all the outgoing waves need be tracked.

9. Interactions of Tracked Waves

A main problem in the method of front tracking is the interaction of tracked waves. These interactions include the collision and scattering of

curves or nodes, and bifurcations in the local wave structure about a node such as a transition from regular to Mach reflection. This section describes some ideas that are used for the numerical simulation of interactions between tracked waves. No attempt is made to address the general problem of tracked wave interactions. Instead, some ideas for the detection and identification of wave interactions are sketched, and some special cases that arise in the Richtmyer–Meshkov simulations of the next section are described.

The resolution of a tracked wave interaction consists of detecting an interaction, constructing an approximate solution of an associated 2-dimensional Riemann problem, and the insertion of this solution into the tracked data structures.

Wave interactions in the front tracking method are detected in one of three ways:

1. a bifurcation in the elementary wave associated with the given node,
2. the detection during the propagation of a node of its interaction with other nodes,
3. the occurrence of intersections at non-node points of tracked curves.

Interactions of the first type are identified by a loss of existence of the solution to the steady state Riemann problem associated with the elementary wave or by the explicit inclusion of some bifurcation criterion in the shock polar analysis. Their resolution consists of determining (or approximating) the scattered wave structure produced by the bifurcation and adapting the tracked wave structures to appropriately model the bifurcated wave.

Interactions of the second type are detected during the calculation of the new node position. If the incoming curves are short, they may propagate completely past each other during a single time step. This means that the nodes at opposite ends of the incoming curves collided at some intermediate time between the beginning and end of the time step. Since the detection of a node interaction may depend on the order in which the nodes are propagated, when a wave interaction is detected at a node, that node is left unpropagated and is moved to the end of the list of nodes being propagated. The propagation of other nodes is continued. If an interaction is again detected when that node is propagated a second time, it along with any other nodes that interact with it are stored in a data structure for further processing. The relation of node interaction is transitive so overlapping sets of interacting nodes are merged.

A set of interacting nodes defines an associated 2-dimensional Riemann problem. The tracked curves at the interacting nodes are of two types, those

internal to the interaction (internal null curves) and those connected to the exterior of the region of interaction (external curves). Conceptually, at an intermediate time between t and $t + \Delta t$ the interacting nodes and internal curves collapse onto a single point that can be regarded as the "node" of the external curves. The local data at this "node" defines the associated 2-dimensional Riemann problem. Since the data for this 2-dimensional Riemann problem need not be a perturbation of an elementary wave, this pseudo node may be unstable and immediately bifurcate and scatter into a set of outgoing nodes and curves.

Interactions of the third type are called tangles. Tangles occur when two or more curves cross each other during a single time step. Tangles differ from the previous two classes primarily in that they occur in the interior of curves rather than at the nodes. They are detected at the end of the propagation of the tracked front, when the tracked curves are tested for self-intersections at non-nodal points. The resolution of tangles is similar to the solution of the other two classes. A discussion of the untangling of tracked scalar waves (contact discontinuities in hydrodynamics) can be found in [16].

The wave patterns produced by the interactions discussed above can be complicated [4]. If (7.1) reduces to a single scalar equation, an exact analytic solution to the 2-dimensional Riemann problem can often be described [21, 22, 30]. Also for a given class of simulations it is possible to identify the types of bifurcations that will occur, so a general solution to the 2-dimensional Riemann problem is not needed. Nor is an exact solution to a particular tracked wave interaction always necessary. Usually only the strongest waves in the solution are tracked. The weaker waves are then captured by the interior solver. This is an important point since the partial tracking helps control the geometric complexity of the tracked waves and allows greater flexibility in the approximation of interactions where the exact solution is complicated or unknown.

In the Richtmyer–Meshkov simulations described in the next section, only two classes of physical bifurcations occur. These are the initial production of the diffracted waves when the shock first reaches the fluid interface and the scattering of two shock diffraction nodes on their collision. Theorem 3 ensures that no additional bifurcations occur in the shock diffraction regime if the amplitude of the perturbation of the contact is not too large.

Figure 9.1 describes the approximate solution of the shock–contact tangle. The point of intersection between the two waves are replaced by a pair of nodes corresponding to the regular diffraction of the two waves. These two nodes are connected by a common set of outgoing waves corresponding to the transmitted shock wave, the deflected contact, and the reflected wave. The two nodes subsequently propagate away from each

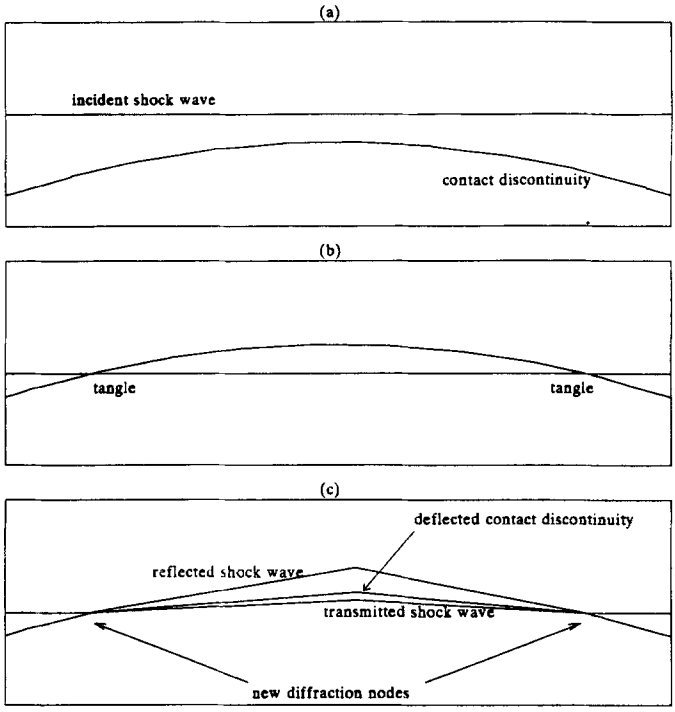

FIG. 9.1. A shock wave and contact discontinuity tangle. Figure 9.1a shows the two curves at the beginning of the time step. Since the two curves are propagated independently, it is possible for intersections to form during propagation. Any intersections are detected at the end of the front propagation. Once the interaction is identified as a shock wave–contact discontinuity collision, new nodes are inserted at the points of intersection. The reflected and transmitted waves together with the deflected contact are installed at the new nodes. The positions of the new nodes corresponds to the intersections shown in Fig. 9.1b.

other in opposite directions from the point of the initial shock–contact collision.

Figure 9.2 shows the approximate resolution of the collision of two diffraction nodes. The two nodes have a common incident shock and propagate towards each other along the same contact discontinuity. During the time step with the interaction, the incident shock moves completely past the incoming contact discontinuity, the transmitted and reflected waves separate from the deflected contact and begin to propagate away from each other. The exact solution to this interaction is complicated. The pair of transmitted shocks reflect off each other producing a pair of Mach triple points propagating away from each other along each transmitted wave. Similarly for the pair of reflected shocks. The reflected waves and slip lines

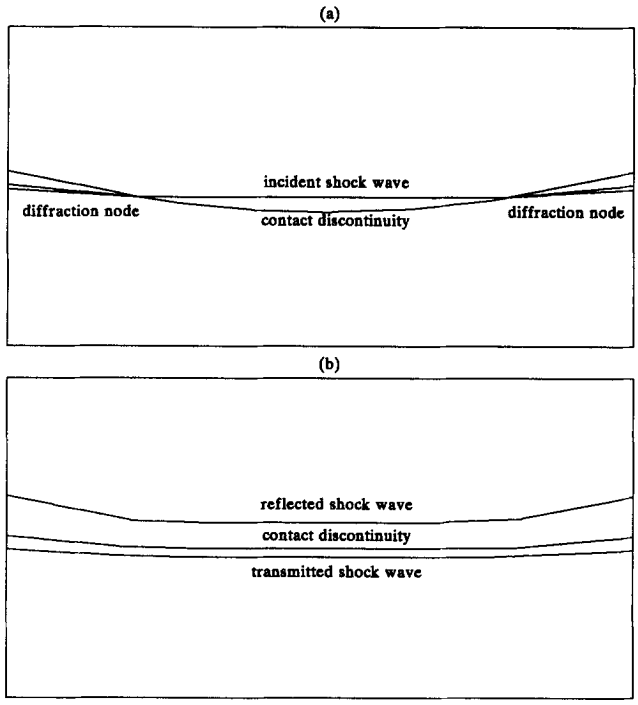

FIG. 9.2. The collision of two regular diffraction nodes. Figure 9.2a shows the tracked wave configuration at the beginning of the time step and Fig. 9.2b shows the tracked waves after the resolution of the interaction. The two diffraction nodes are propagating towards each other. The incident shock wave moves completely past the ahead contact discontinuity during the time Δt, resulting in the collision of the two diffraction nodes. The approximate solution joins the two pairs of reflected and transmitted shock waves and removes the two diffraction nodes. The reflected and transmitted shocks "lift" off the contact discontinuity curve and begin to propagate away from each other.

from the four Mach nodes in turn interact with the contact discontinuity from which the two pairs of shocks have just exited. However, the secondary waves produced by the Mach triple points are weak enough so that they need not be tracked. The solution is approximated by simply joining the reflected and transmitted waves into a pair of waves on opposite sides of the original contact discontinuity. This is equivalent to not tracking the waves transverse to the main front near the interaction.

10. NUMERICAL RESULTS

The number and types of the unstable modes that are observed in the Richtmyer–Meshkov instability depends on many parameters. These in-

clude the incident shock strength, the initial geometry of the two waves, and the physical properties of the gases. A single mode can be isolated when the incident shock wave is planar and the contact discontinuity has the shape of a single period sine curve. More complicated geometries for the initial gas interface can be used to study the interaction between different unstable modes. The fluid interfaces considered below include boundaries between two regions of the same gas at different temperatures, and boundaries between two different gases with different equations of state. Some particularly interesting wave structure is observed when a shock incident in air

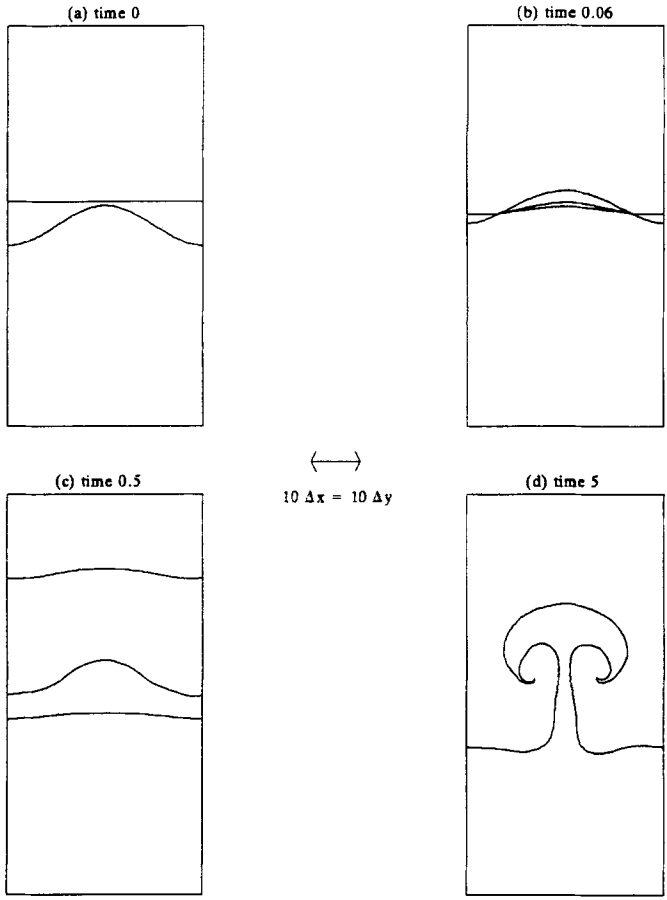

FIG. 10.1. A shock hitting a contact discontinuity separating two masses of air at different temperatures. The pressure ratio across the shock is 100 and the density ratio across the contact discontinuity is 2.86. The shock is incident in the lighter gas. The grid is 40 × 80.

collides with an interface between air and the highly compressible gas sulphur hexafluoride. As the incident shock passes through the air–SF_6 interface, the transmitted shock wave is nearly contiguous with the deflected gas interface.

In all the simulations described below, the side boundary conditions are periodic, and the upper and lower are Dirichlet. The gases are modeled using the polytropic (gamma law) equation of state, but other equations of states are currently being implemented.

Figure 10.1 shows a series of frames documenting the growth of a single unstable finger in an air to air interface with $\gamma = 1.4$. The shock wave is

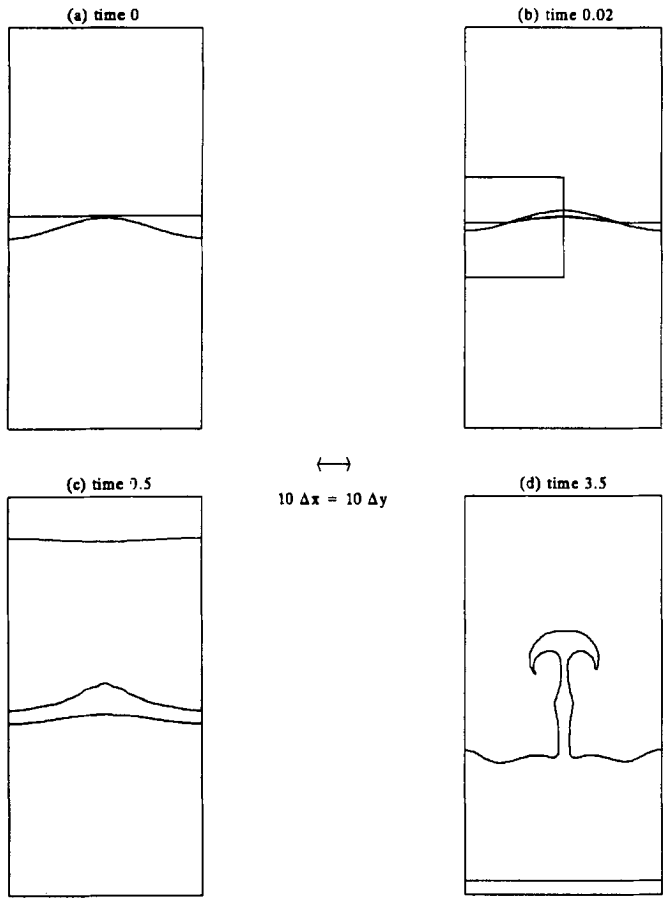

FIG. 10.2. A shock hitting a contact discontinuity separating air from SF_6. The contact discontinuity curve is given an initial shape of a sine curve. The shock is incident from the air and has a pressure ratio of 10. The grid is 60 × 120. The boxed region in Fig. 10.2b is blown up in the next figure.

incident in the lighter (warmer) air and the ratio of the pressure behind the shock to the pressure in front is 100. Initially the cooler air is about 2.86 times as dense as the lighter air. A net vertical velocity is given to the initial contact discontinuity to keep the unstable interface centered in the computational domain.

The gas interface is first flattened by the incident shock wave. The diffraction of the shock wave through the interface cause the reflected and transmitted shocks to assume the geometry of the original interface. As the waves begin to propagate away from each other, the unstable mode in the contact discontinuity grows, and the two shock waves restabilize to planar

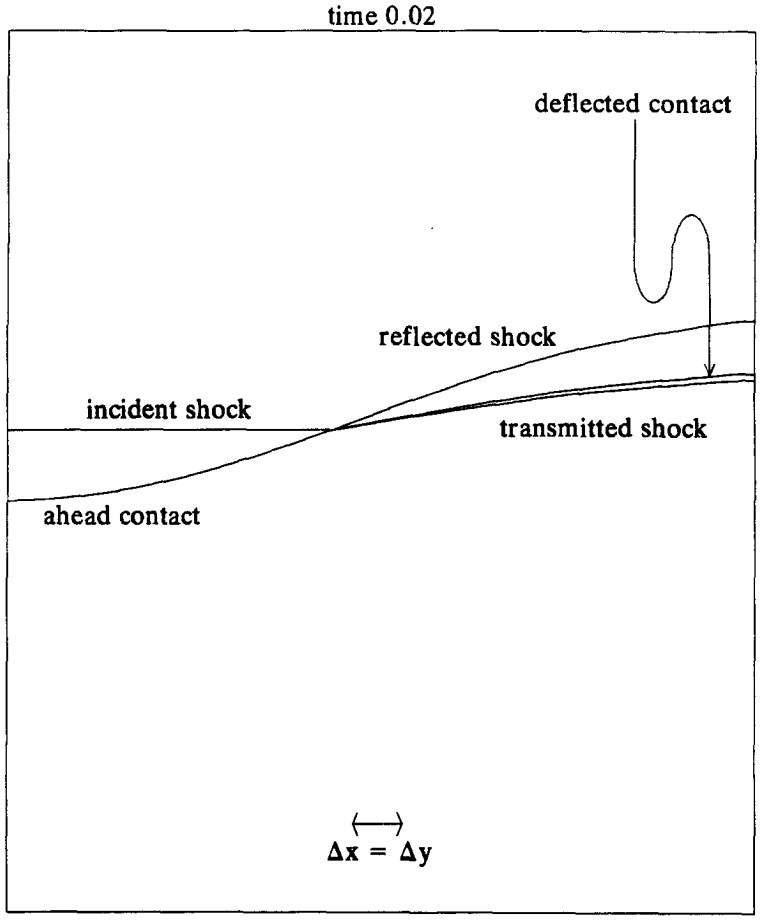

FIG. 10.3. A blowup of a subregion of Fig. 10.2b showing the incident shock colliding with the ahead contact discontinuity, producing reflected and transmitted shocks.

curves. The shocks eventually exit the open boundaries leaving the contact discontinuity as the only tracked wave.

Figure 10.2 shows a similar development of an unstable finger, except here the gas interface separates air ($\gamma = 1.4$) from sulphur hexafluoride ($\gamma = 1.094$).The pressure ratio across the incident shock is 10. At room temperature, SF_6 is about 5.03 times as dense as air. The simulation points out a unique capability of the front tracking method. During the diffraction, the angle between the transmitted shock and the deflected contact at the node is less than 1°, and the two waves are nearly contiguous, Fig. 10.3.

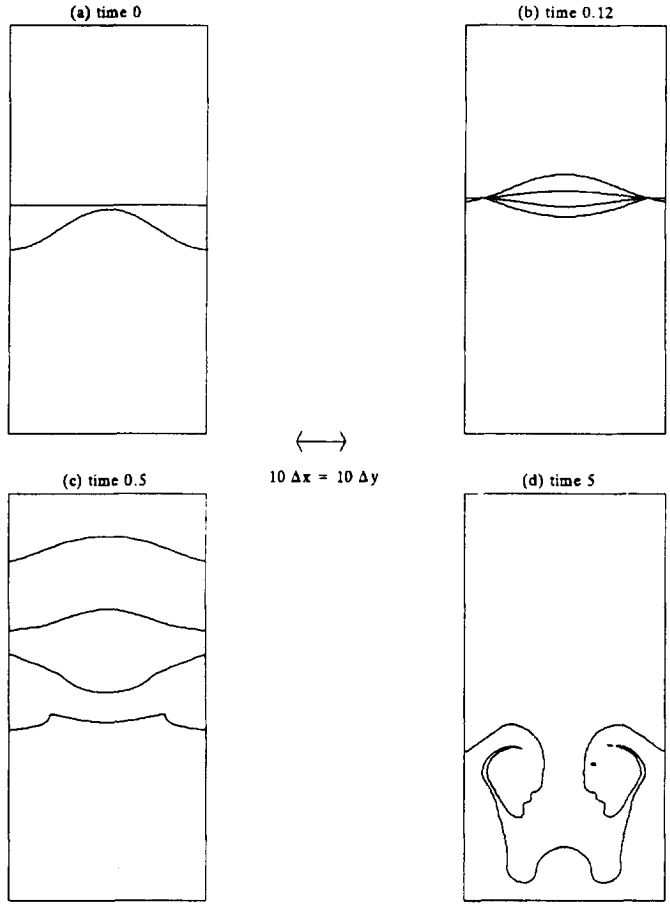

FIG. 10.4. A shock–contact interaction that produces a reflected Prandtl–Meyer rarefaction wave. The pressure ratio across the shock is 100 and the density ratio across the contact discontinuity is 10. Both gases are polytropic with $\gamma = 1.4$. The shock wave is incident in the heavier gas and the grid is 40×80.

In Figure 10.4 a shock-contact interaction is shown where the shock is incident in the heavy gas. The reflected wave here is a Prandtl–Meyer rarefaction, the two leading edges of which are tracked. The pressure ratio across the incident shock is 100, and the heavy gas is 10 times as dense as the lighter gas. Note that the phase of the fluid interface is reversed by this diffraction, an effect typical for interactions where the shock is incident in the fluid with the slower sound speed. Figure 10.4c shows the waves shortly after the incident shock has completely diffracted through the interface. The two kinks on the transmitted shock are points of Mach reflection caused by

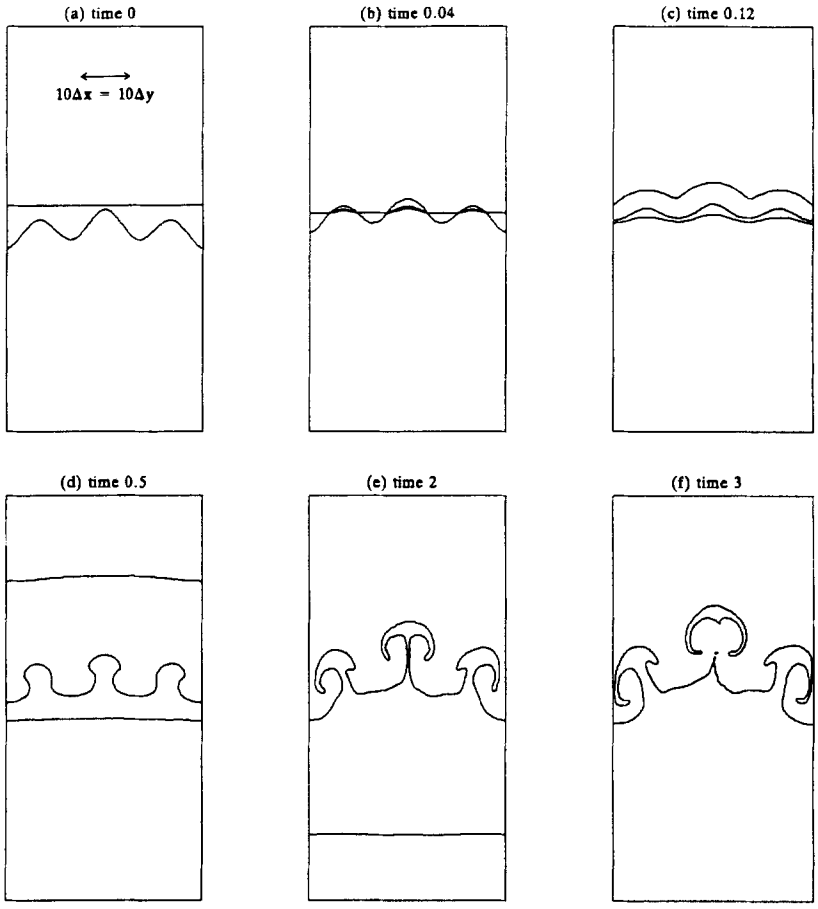

FIG. 10.5. A series of frames showing a shock–contact interaction with three unstable modes. Both gases are polytropic with $\gamma = 1.4$. The pressure ratio across the incident shock is 100, and the density ratio (above to below) across the original contact is 2.86. The grid is 40×80.

the interaction of the two diffraction nodes across the periodic boundary. As mentioned above the waves produced by this secondary interaction are untracked. The long time development of the surface instability is shown in Fig. 10.4d. An interesting feature of this figure is the development of the dimple in the spike. There was some question whether this dimple was a result of the untracked transverse waves along the transmitted shock, or by reflections from the boundaries because of an incomplete implementation of the flow-through boundary conditions. The flow-through boundary conditions are obtained by the first-order method of extrapolating the interior states near the boundaries into the exterior. Experience shows that the

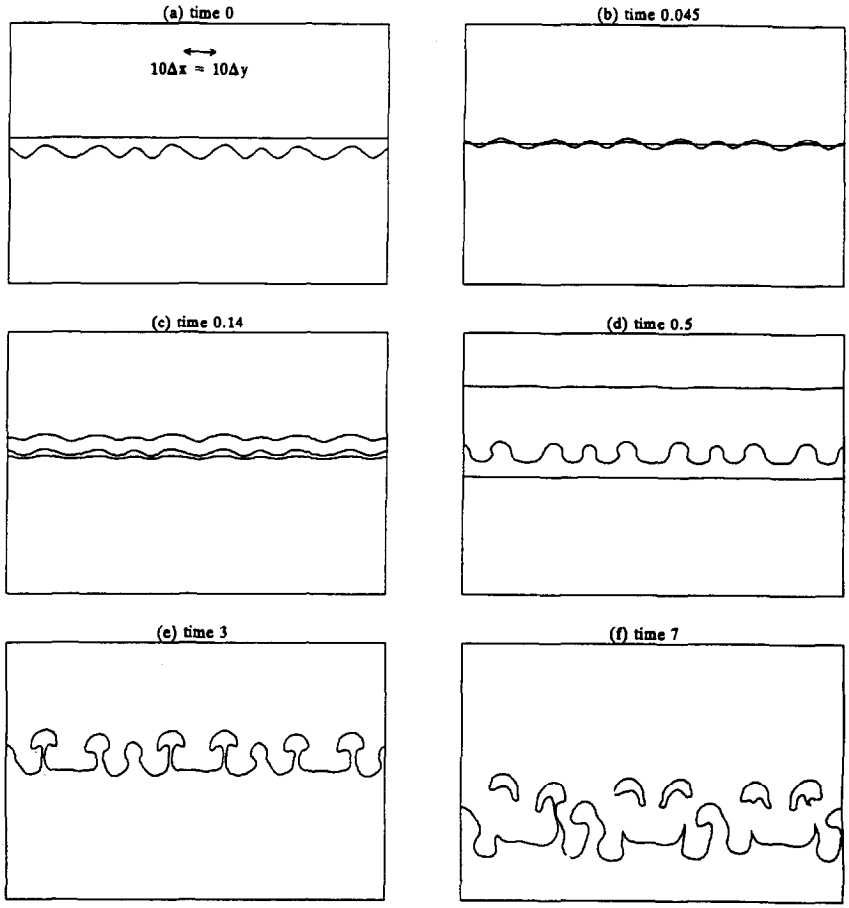

FIG. 10.6. A series of frames showing a shock–contact interaction with several modes. Both gases are polytropic with $\gamma = 1.4$. The pressure ratio across the incident shock is 100, and the density ratio (above to below) across the original contact is 2.86. The grid is 120×80.

reflected signals produced by this form of the flow-through boundary conditions are small but non-zero, and thus might be a factor in the generation of the secondary instability seen in the spike. To investigate this question, the simulation shown in Fig. 10.4 was rerun using a computational domain three times as long in the vertical direction. The results were nearly identical. This suggests that the dimple is a result of the transverse wave interactions and not a result of the boundary conditions.

In addition to calculations of the growth of a single finger, simulations that involve several unstable modes have also been performed. Figures 10.5 and 10.6 use the same basic setup as Fig. 10.1, except that the initial gas

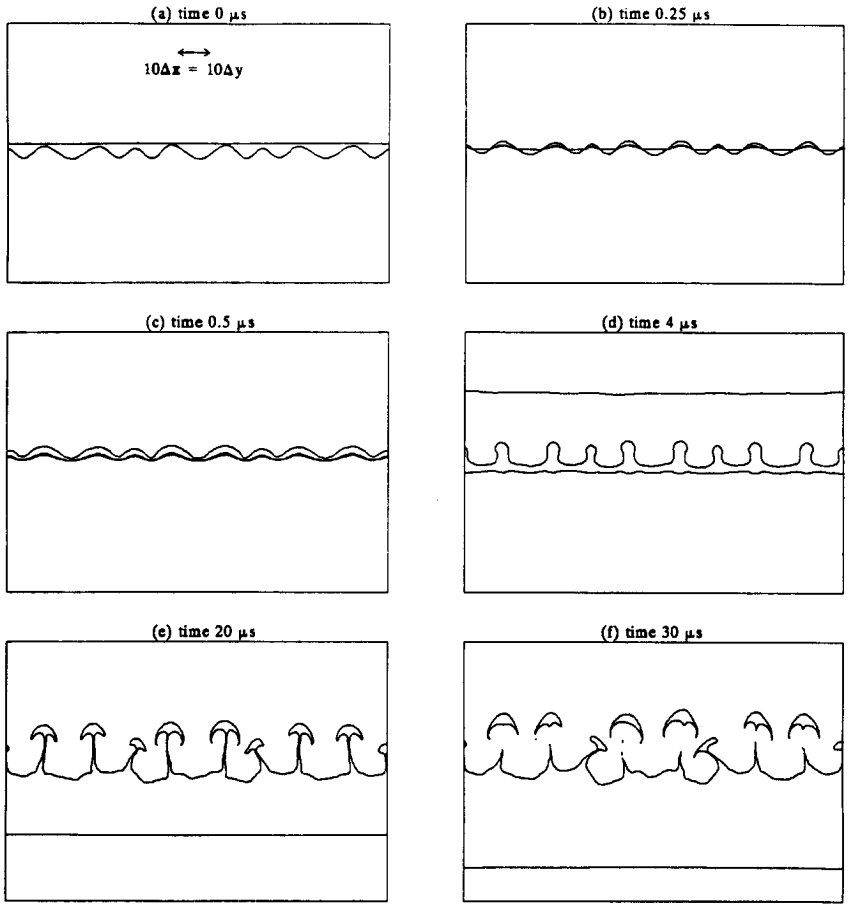

FIG. 10.7. A series of frames showing a shock in helium ($\gamma = 1.63$) colliding with an air ($\gamma = 1.4$)–helium interface. The pressure in front of the shock is 1 atm, and the pressure behind is 1000 atm. The density of dry air at 25°C is 0.00118497 g/cc and the density of helium at the same temperature is 0.000101325 g/cc. The grid is 120 × 80.

interface is given a more complicated geometry. Figure 10.7 shows the interaction of a shock wave incident in helium ($\gamma = 1.63$) with a helium to air interface.

11. Conclusions

It has been seen that the interaction of a shock wave with a fluid interface is properly studied in the context of a supersonic steady state Riemann problem. The small incident angle asymptotics of this interaction lead to a corresponding 1-dimensional unsteady Riemann problem.

These results show that front tracking offers a useful method for the simulation of shock wave–contact discontinuity interactions. It allows for a sharp resolution of the diffracted wave patterns produced by the interaction of the two waves and a clear picture of the growth of unstable modes in the gas interface.

The framework for the resolution of tracked wave interactions has been shown to be capable of handling complicated situations. Furthermore, it is possible to include new bifurcations as they are needed or to remove tracking when the result of a wave interaction is either too complicated or unknown.

Acknowledgments

Thanks are given to Professor James Glimm for his encouragement of this work and special thanks are given to Dr. Ralph Menikoff and Professor Bradley J. Plohr for helpful discussions.

References

1. A. M. Abd-El-Fattah and L. F. Henderson, Shock waves at a fast–slow gas interface, *J. Fluid Mech.* **86** (1978), 15.
2. A. M. Abd-El-Fattah and L. F. Henderson, Shock waves at a slow–fast gas interface, *J. Fluid Mech.* **89** (1978), 79.
3. L. F. Henderson, The refraction of a plane shock wave at a gas interface, *J. Fluid Mech.* **26** (1966), 607.
4. R. G. Jahn, The refraction of shock waves at a gaseous interface, *J. Fluid Mech.* **1** (1956), 457.
5. A. M. Abd-El-Fattah, L. F. Henderson, and A. Lozzi, Precursor shock waves at a slow–fast gas interface, *J. Fluid Mech.* **76** (1976), 157.
6. V. Andronov, S. M. Bakhrakh, E. E. Meshkov, V. N. Mokhov, V. V. Nikiforov, A. V. Pevnitskii, and A. I. Tolshmyakov, *Soviet Phys. JETP* **44** (1967), 424–427.
7. H. A. Bethe, "The Theory of Shock Waves for an Arbitrary Equation of State," Report PB-32189, Clearinghouse for Federal Scientific and Technical Information, U.S. Dept. of Commerce, Washington DC, 1942.
8. I. L. Chern, J. Glimm, O. McBryan, B. Plohr, and S. Yaniv, Front tracking for gas dynamics, *J. Comput. Phys.* **62** (1986), 83–110.
9. R. Courant and K. O. Friedrichs, "Supersonic Flow and Shock Waves," Springer-Verlag, New York, 1948.

10. J. GLIMM AND D. H. SHARP, "Elementary Waves for Hyperbolic Equations in Higher Space Dimensions: An Example from Petroleum Reservoir Modeling," DOE Research and Development Report DOE/ER/03077-248, 1985.
11. J. GLIMM AND D. H. SHARP, An S matrix theory for classical nonlinear physics, *Found. Phys. B* **16** (1986), 125–141.
12. J. GLIMM, E. ISAACSON, D. MARCHESIN, AND O. MCBRYAN, Front tracking for hyperbolic systems, *Adv. in Appl. Math.* **2** (1981), 91–119.
13. J. GLIMM AND O. MCBRYAN, A computational model for interfaces, *Adv. in Appl. Math.* **6** (1985), 422–435.
14. J. GLIMM, C. KLINGENBERG, O. MCBRYAN, B. PLOHR, D. SHARP, AND S. YANIV, Front tracking and two-dimensional Riemann problems, *Adv. in Appl. Math.* **6** (1985), 259–290.
15. J. GLIMM, J. GROVE, AND X. L. LI, Three remarks on the front tracking method, *in* "Proceedings, Conference in Taormina, Sicily, 1987."
16. J. GLIMM, J. GROVE, B. LINDQUIST, O. A. MCBRYAN, AND G. TRYGGVASON, The bifurcation of tracked scalar waves, *SIAM J. Sci. Statist. Comput.* **9**, No. 1 (1988).
17. C. W. HIRT AND B. D. NICHOLS, Volume of fluid (VOF) method for the dynamics of free boundaries, *J. Comput. Phys.* **39** (1981), 201–225.
18. P. LAX, Hyperbolic systems of conservation laws II, *Comm. Pure Appl. Math.* **10** (1957), 537–566.
19. B. VAN LEER, Toward the ultimate conservative difference scheme. IV. A new approach to numerical convection, *J. Comput. Phys.* **23** (1977), 276–299.
20. B. VAN LEER, Towards the ultimate conservative difference scheme. V. A second-order sequel to Godunov's method, *J. Comput. Phys.* **32** (1977), 101–136.
21. W. B. LINDQUIST, Construction of solutions for two dimensional Riemann problems, *Comput. Math. Appl. A* **12**, No. 4/5 (1986), 615–630.
22. W. B. LINDQUIST, The scalar Riemann problem in two spatial dimensions: Sufficiency condition for piecewise smoothness of solutions and its breakdown, *SIAM, J. Math. Anal.*, Vol. 17, No. 5, Sept. 1986.
23. R. MENIKOFF AND B. J. PLOHR, "Riemann Problem for Fluid Flow of Real Materials," Report LA-UR-87-2259, Los Alamos.
24. W. F. NOH AND P. WOODWARD, SLIC (simple line interface calculation), *in* "Lecture Notes in Physics Vol. 59," Springer-Verlag, New York, 1976.
25. J. D. RAMSHAW AND J. A. TRAPP, A numerical technique for low-speed homogeneous two-phase flows with sharp interfaces, *J. Comput. Phys.* **21** (1976), 438–453.
26. R. D. RICHTMYER, Taylor instability in shock acceleration of compressible fluids, *Comm. Pure Appl. Math.* **13** (1960), 297–319.
27. R. G. SMITH, The Riemann problem in gas dynamics, *Trans. Amer. Math. Soc.* **249** (1979), 1–50.
28. P. A. THOMPSON, A fundamental derivative in gasdynamics, *Phys. Fluids* **14**, No. 9 (1971), 1843–1849.
29. P. A. THOMPSON, "Compressible-Fluid Dynamics," pp. 252–254, McGraw–Hill, New York, 1972.
30. D. WAGNER, The Riemann problem in two space dimensions for a single conservation law, *SIAM, J. Math. Anal.* **14**, No. 3 (1983), 534–559.
31. H. WEYL, Shock waves in arbitrary fluids, *Comm. Pure Appl. Math.* **2** (1949), 103–122.
32. A. H. WILSON, "Thermodynamics and Statistical Mechanics," pp. 56–60, Cambridge Univ. Press, Cambridge, 1957.
33. D. L. YOUNGS, Time-dependent multi-material flow with large fluid distortion, *in* "Numerical Methods for Fluid Dynamics" (M. J. Baines, Ed.) Academic Press, New York, 1982.
34. D. L. YOUNGS, Numerical simulation of turbulent mixing by Rayleigh–Taylor instability, *Physica D* **12** (1984), 32–34.